Principal frequency, superbandwidth, and low-order harmonics generated by superoscillatory pulses

Enrique G. Neyra [1,*] Demian A. Biasetti,[1] Fabián Videla [1,2] Lorena Rebón [3,4] and Marcelo F. Ciappina [5,6,7,†]

[1]*Centro de Investigaciones Ópticas (CICBA-CONICET-UNLP), Cno. Parque Centenario y 506, P.O. Box 3, 1897 Gonnet, Argentina*
[2]*Departamento de Ciencias Básicas, Facultad de Ingeniería UNLP, 1 y 47 La Plata, Argentina*
[3]*Departamento de Física, FCE, Universidad Nacional de La Plata, C.C. 67, 1900 La Plata, Argentina*
[4]*Instituto de Física de La Plata, CONICET, Diag. 113 e/ 63 y 64, La Plata, 1900, Argentina*
[5]*Physics Program, Guangdong Technion – Israel Institute of Technology, Shantou, Guangdong 515063, China*
[6]*Technion – Israel Institute of Technology, Haifa, 32000, Israel*
[7]*Guangdong Provincial Key Laboratory of Materials and Technologies for Energy Conversion, Guangdong Technion – Israel Institute of Technology, Shantou, Guangdong 515063, China*

(Received 30 May 2022; accepted 7 September 2022; published 30 September 2022)

An alternative definition to the main frequency of an ultrashort laser pulse, named principal frequency (ω_P), was recently introduced in E. G. Neyra *et al.* [Phys. Rev. A **103**, 053124 (2021)], resulting in a more transparent description of the nonlinear dynamics of a system driven by this coherent source. In this paper, we extend the definition of ω_P incorporating the spectral phase of the pulse. This upgraded definition allow us to deal with superoscillatory pulses as well as to characterize subcycle pulses with a complex spectral content. Simultaneously, we study the nonlinear interaction between a few-cycle superoscillatory pulse with a gaseous system, analyzing the spectral characteristics of the fundamental, third, and fifth harmonics. Here, we make use of an *ab initio* quantum mechanical approach, supplemented with a wavelet analysis. We show that the spectral characteristics of the low-order harmonics are very well explained in terms of ω_P, as well as the effective bandwidth of the superoscillatory pulse. Our findings reinforce previous results that showed an increase of the effective bandwidth in the superoscillatory region and the possibility to generate unique frequencies by a linear synthesis. We thus open not only perspectives in ultrafast optics, exploring pathways toward the generation of fully tunable strong and short coherent sources, but also discuss possible extensions of the concepts presented here to other wave phenomena that can be found in acoustics, signal processing, and quantum mechanics.

DOI: 10.1103/PhysRevResearch.4.033254

I. INTRODUCTION

The possibility to create and manipulate few-cycle ultrashort laser pulses in the visible, infrared, and XUV spectral ranges has led to numerous studies in the field of laser-matter interaction, where this type of pulse finds diverse applications [1–4]. For instance, the interest in these pulses covers different topics, including the manipulation of the quantum properties of physical systems [5–7], the study of the temporal dynamics of the chemical reactions [8,9], and the laser-matter interaction in the strong-field regime [10].

Since the amplitude of the electric field varies within an optical cycle, the nonlinear matter interaction processes driven by few-cycle laser pulses are strongly dependent on the carrier-envelope phase. This quantity plays an instrumental role in, for example, the high-order harmonic generation (HHG) phenomenon. This matter has been widely studied since the early days (see, e.g., Ref. [11] and references therein). Beyond this fact, we have recently showed in Ref. [12] that, in the few-cycle regime, the frequency that dominates the nonlinear matter interactions undergoes a small shift to frequencies higher than the carrier frequency of the pulse, ω_0, usually considered the main frequency to describe every nonlinear phenomena. This shift in the value of the main frequency is well represented by the so-called *principal frequency*, ω_P, a concept introduced in our previous work. According to its definition, ω_P corresponds to an increase with respect to the carrier frequency that depends on the bandwidth $\Delta\omega$ of the given pulse, i.e., $\omega_P = \omega_P(\omega_0, \Delta\omega)$.

On the other hand, recently there has been a great deal of interest in the study of the low-order harmonics generation (LHG). Here, the so-called near-threshold harmonics can be considered the most relevant ones. Their significance lies principally in the possibility to generate coherent light sources with a high repetition rate and efficiency [13,14]. While HHG is a well-understood phenomenon, the theoretical description of LHG is rather more complicated and not exempt of controversies [15,16]. Generally, it can be thought that the LHG can be explained by invoking the perturbation theory,

*enriquen@ciop.unlp.edu.ar
†marcelo.ciappina@gtiit.edu.cn

meanwhile the usual HHG can be described by applying semiclassical arguments, e.g., HHG is well understood employing the three-step model [17]. When comparing with experimental measurements, however, one finds that it is difficult to give a solid theoretical description for the LHG. First, perturbation theory is unsuitable when the driving laser is sufficiently intense. Second, due to the important roles played by both the Coulomb potential and the bound excited states, methods such as the strong field approximation, which (i) neglects the Coulomb potential in different parts of the description and (ii) only takes into account the ground state of the system, cannot be directly used to describe the LHG. Thus, full quantum mechanical models, jointly with those where the Coulomb potential is included, appear to be the most suitable ones to theoretically describe the underlying physics behind the LHG [18,19].

In parallel, the phenomenon of superoscillations, mathematically described by a band-limited function that can oscillate, locally, with a frequency higher than the highest frequency of its Fourier spectrum [20,21], has raised a great deal of physical and mathematical interesting and intriguing implications [22–28]. Indeed, in Ref. [29], we have shown that the superoscillatory (SO) phenomenon is also represented by laser pulses with a *superbandwidth*. When applied to a two-level system, and within the time window where the superoscillation occurs, these pulses exhibit an effective bandwidth broader than the one fixed by the Fourier transform, which can open unique ways in coherent control [30,31] or in ultrafast spectroscopy.

In this paper, we start by extending the definition of the principal frequency, ω_P, to take into account the spectral phase of the pulse, $\Phi(\omega)$. We show that this upgraded definition gives a more appropriate description of the main spectral contribution of SO pulses. In addition, we show that the same definition also allows a clearer description of the main frequency of subcycle pulses, with a very complex spectral content, like the one synthesized in Refs. [32,33]: The so-called *optical attosecond pulses* or *field transients*. Finally, we numerically study the bound-electron nonlinear response of a gaseous system driven by a SO pulse, which can be implemented by means of an interferometric system. The study is carried out through the one-dimensional time-dependent Schrödinger equation (1D-TDSE) in an hydrogen atom. In particular, the spectral characteristics of the fundamental, third, and fifth harmonics, in the temporal window where the pulse is SO, were obtained through a wavelet analysis, from which we can conclude that the spectral features of these harmonics, i.e., their bandwidth and main frequency, are very well explained in terms of the superbandwidth of the SO pulses and the extended definition of the principal frequency.

II. PRINCIPAL FREQUENCY

We start by briefly discussing the alternative definition of the main frequency of an ultrashort laser pulse that we introduced in Ref. [12]. Let us take the time-dependent electric field $E(t)$ of such a pulse, and its complex representation in the frequency domain $\tilde{E}(\omega) = \mathcal{F}[E(t)] = |\tilde{E}(\omega)|e^{i\Phi(\omega)}e^{i\phi}$, given by the Fourier transform $\mathcal{F}$, where $|\tilde{E}(\omega)|$ and $\Phi(\omega)$ are the spectral amplitude and phase, respectively, and ϕ is a global phase. That frequency, which we have called the *principal frequency* and denoted as ω_P, is defined by the expression

$$\omega_P = \frac{\int \omega^2 S(\omega) d\omega}{\int \omega S(\omega) d\omega}, \tag{1}$$

where $S(\omega) = |\tilde{E}(\omega)|^2$ is the spectral power. Equation (1) can be seen as the mean of the spectral content of the laser pulse, weighted with a particular density function, $\rho_P(\omega) = \omega S(\omega)$. In our previous work [12], we have shown that ω_P is related with the position of the maxima of $E(t)$, while the standard definition of the main frequency $\omega_0 = \frac{\int \omega S(\omega) d\omega}{\int S(\omega) d\omega}$ [34], is related with its zeros. This means that ω_P will offer a better description of the laser-matter interaction in the nonlinear regime, where the response of the system is led by some power of the peak field amplitude, $(E_0)^n$. However, a nonzero value of the difference $\omega_P - \omega_0$ can only be observed in the few-cycle pulse regime, where the envelope of the field changes significantly in an optical cycle. Furthermore, this difference becomes even larger for single-cycle and subcycle pulses (the latter are also called field transients).

It is evident that the definitions of both ω_0 and ω_P only take into account the spectral power $S(\omega)$ of the pulse and neglects its spectral phase $\Phi(\omega)$, which may be relevant in many cases. In particular, in the SO phenomenon, which has an interferometric origin, the $\Phi(\omega)$ becomes instrumental. In this context, we introduce here an extended version of the principal frequency ω_P, by considering in Eq. (1) the field $\tilde{E}(\omega)$ itself instead of the spectral power $S(\omega)$,

$$\omega_{P_\Phi} \equiv \frac{\int \omega^2 |\tilde{E}(\omega)| e^{i\Phi(\omega)} d\omega}{\int \omega |\tilde{E}(\omega)| e^{i\Phi(\omega)} d\omega}, \tag{2}$$

where the global phase ϕ was trivially canceled as it does not depend on ω. Hence, we can understand the term $\rho_{P_\Phi}(\omega) = \omega|\tilde{E}(\omega)|e^{i\Phi(\omega)}$ in Eq. (2) as a modified density function with respect to the one originally defined by Eq. (1), which is now a complex-valued function. Consequently, ω_{P_Φ} becomes also a complex quantity.

In the following, we apply this definition of the principal frequency ω_{P_Φ} to some examples of SO functions as well as to describe the main frequency of an optical attosecond pulse.

A. Super-oscillatory functions

As a first example, we analyze one of the best-known SO functions, exhaustively studied in Refs. [20,21] and experimentally synthesized in an ultrashort laser pulse in Ref. [35]. That SO field is described by the expression

$$E_1(t) = E_0\left[\cos\left(\frac{\omega_f t}{N}\right) + ia\sin\left(\frac{\omega_f t}{N}\right)\right]^N e^{i\phi}, \tag{3}$$

where N is a positive integer, a is a real value greater than 1, and ω_f is the limit frequency of the Fourier spectrum, i.e., the frequency of the field when $\{N, a\} \to \{1, 1\}$. For simplicity, in the following we normalize the amplitude of the field, setting its maximum value at $E_0 = 1$. The SO behavior is given by the fact that $E_1(t) \approx e^{ia\omega_f t}$, when $N \gg 1$ and for values of $|\omega_f t|/\sqrt{N}$ small enough, that is, in the central region, $E_1(t)$ oscillates with a frequency $\omega_{SO} = a\omega_f > \omega_f$.

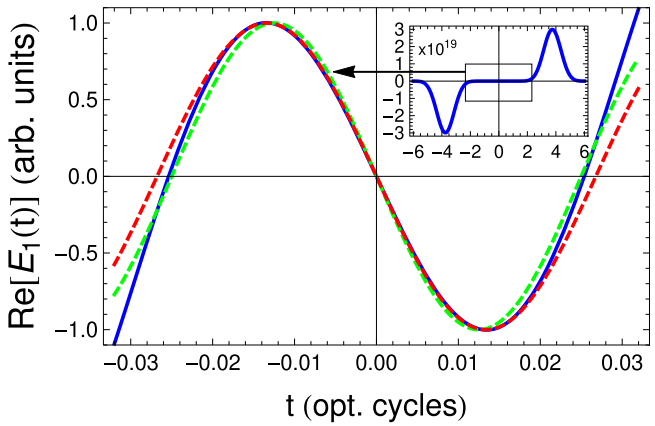

FIG. 1. Comparison between the SO pulse $E_1(t)$ (blue line) and sine waves of frequencies ω_{SO} (green dashed line) and ω_{P1_Φ} (red dashed line) in the SO region (the central part of the pulse). In the inset plot, we show the real part of $E_1(t)$ over several optical cycles ($2\pi/\omega_f$) of the sine waves for setting values $a = 20$ and $N = 15$.

In the frequency domain, the expression in Eq. (3) is a sum of Dirac delta functions:

$$\tilde{E}_1(\omega) = e^{i\phi} \sum_{j=0}^{N} C_j(N,a) \times \delta(\omega - \omega_j(N)), \tag{4}$$

where the discrete frequencies are given by $\omega_j(N) = (1 - \frac{2j}{N})\omega_f$, with Fourier coefficients $C_j(N,a) = \binom{N}{j}(\frac{1+a}{2})^{N-j}(\frac{1-a}{2})^j$. Then, the frequency ω_{P_Φ} defined by Eq. (2) can be written as

$$\omega_{P1_\Phi}(N,a) = \frac{\sum_{j=0}^{N} \omega_j(N)^2 C_j(N,a)}{\sum_{j=0}^{N} \omega_j(N) C_j(N,a)}, \tag{5}$$

resulting in

$$\omega_{P1_\Phi}(N,a) = \left[\frac{1 + a^2(N-1)}{aN}\right]\omega_f. \tag{6}$$

This expression converges to ω_{SO} when $N \to \infty$. Even more, for finite N values, we can numerically demonstrate that $\omega_{P1_\Phi}(N,a)$ allows us to describe the shape of the field in the SO region and localize its peak values (maxima and minima) in a better way than ω_{SO}. This can be observed in Fig. 1, where we show the real part of the field $E_1(t)$ for $\phi = \pi/2$, $a = 20$, and $N = 15$, and a zoomed image of the SO region where, for comparative purposes, we also plotted the harmonic waves oscillating at the SO frequency ω_{SO} (Re[$e^{ia\omega_f t}e^{i\phi}$]) and at the frequency ω_{P1_Φ} (Re[$e^{i\omega_{P1_\Phi} t}e^{i\phi}$]). It should be noted, however, that the position of the zeros of $E_1(t)$ are best described by ω_{SO}. A more complete analysis for different values of parameters a and N can be found in the Appendix.

As a second example, we study the SO functions proposed to obtain subdiffractive Gaussian beams and sub-Fourier ultrashort Gaussian pulses, which, as shown in Refs. [36,37], can be obtained by means of simple interferometric techniques. In the time domain, these SO pulses are the result of the interference between an ultrashort Gaussian pulse, characterized by a central frequency ω_C and a bandwidth $\Delta\omega_2$, and the same pulse modified by a quadratic phase or a *Gaussian filter* [36]. In the first case, a pulse $\tilde{E}_G(\omega) = e^{-(\frac{\omega-\omega_C}{\Delta\omega_2})^2}$ is the input of a Michelson interferometer, with a dispersive media in one of its arms, which introduce a quadratic phase (chirp) to the electric field traveling in that path. After being recombined into a beam splitter with the pulse that travels without modification, we can write the resulting SO field, in the frequency domain, as

$$\tilde{E}_2(\omega) = e^{-(\frac{\omega-\omega_C}{\Delta\omega_2})^2}(1 + \alpha_2 e^{i\theta(\alpha_2,\beta_2)} e^{i\beta(\omega-\omega_C)^2})e^{i\phi}. \tag{7}$$

Here, the value of α_2 indicates the relative amplitude between the pulses in each arm of the interferometer, while β_2 is the quadratic chirp parameter. The condition of purely destructive interference, necessary to obtain SO pulses, can be achieved by controlling α_2 and β_2, and as a consequence, the phase $\theta = \theta(\alpha_2, \beta_2)$ [36].

For the pulse defined in Eq. (7), the exact analytical expression of ω_{P_Φ} is given by

$$\omega_{P2_\Phi} = \omega_C \frac{\left(1 + \frac{\Delta\omega_2^2}{2\omega_C^2}\right)\Theta(\beta_2,\Delta\omega_2) + \alpha_2\, e^{-i\tilde{\theta}(\alpha_2,\beta_2)}\left(1 - \frac{i\Delta\omega_2^2}{2\omega_C^2\Theta(\beta_2,\Delta\omega_2)^2}\right)}{\Theta(\beta_2,\Delta\omega_2) + \alpha_2\, e^{-i\tilde{\theta}(\alpha_2,\beta_2)}}, \tag{8}$$

with $\tilde{\theta}(\alpha_2,\beta_2) = \theta(\alpha_2,\beta_2) + \frac{\pi}{4}$ and $\Theta(\beta_2,\Delta\omega_2) = \sqrt{\beta_2\Delta\omega_2^2 - i}$. It is important to note that, when $\alpha_2 \to 0$, $\tilde{E}_2(\omega)$ approaches the initial Gaussian pulse $\tilde{E}_G(\omega)$, and $\omega_{P2_\Phi} \to \omega_C[1 + \frac{1}{2}(\frac{\Delta\omega_2}{\omega_C})^2]$, which coincides with the expression that is obtained from the original definition of the principal frequency ω_P [Eq. (1)] introduced in Ref. [12], that does not consider the spectral phase of the field.

Alternatively to the previous interferometric system, a SO ultrashort pulse in the few-cycle regime can be synthesized by introducing a filter with a rectangular spectral response in one of the arms of the interferometer, whose input is a sinclike pulse, instead of a Gaussian pulse with a *Gaussian filter* (see, e.g., Ref. [36]). As a consequence, in the frequency domain, the resulting SO pulse is described by the expression

$$\tilde{E}_3(\omega) = \left[\mathrm{rect}\left(\frac{\omega-\omega_C}{\Delta\omega_3}\right) - \alpha_3\,\mathrm{rect}\left(\frac{\omega-\omega_C}{\beta_3\Delta\omega_3}\right)\right]e^{i\phi}, \tag{9}$$

where the initial pulse is represented by a rectangle function centered at the frequency ω_C, with a bandwidth $\Delta\omega_3$, i.e., $\tilde{E}_S(\omega) = \mathrm{rect}(\frac{\omega-\omega_C}{\Delta\omega_3})$. In Eq. (9), α_3 represents the relative amplitude between the pulses that travel through the different arms of the interferometer, just like in the previous interferometric scheme, while the parameter β_3 ($0 < \beta_3 < 1$) is now the filtering parameter. In this case, the purely destructive interference condition is easily reached introducing a π phase between the arms of the interferometer. Therefore, by following the definition in Eq. (2), we can see that ω_{P_Φ} is now

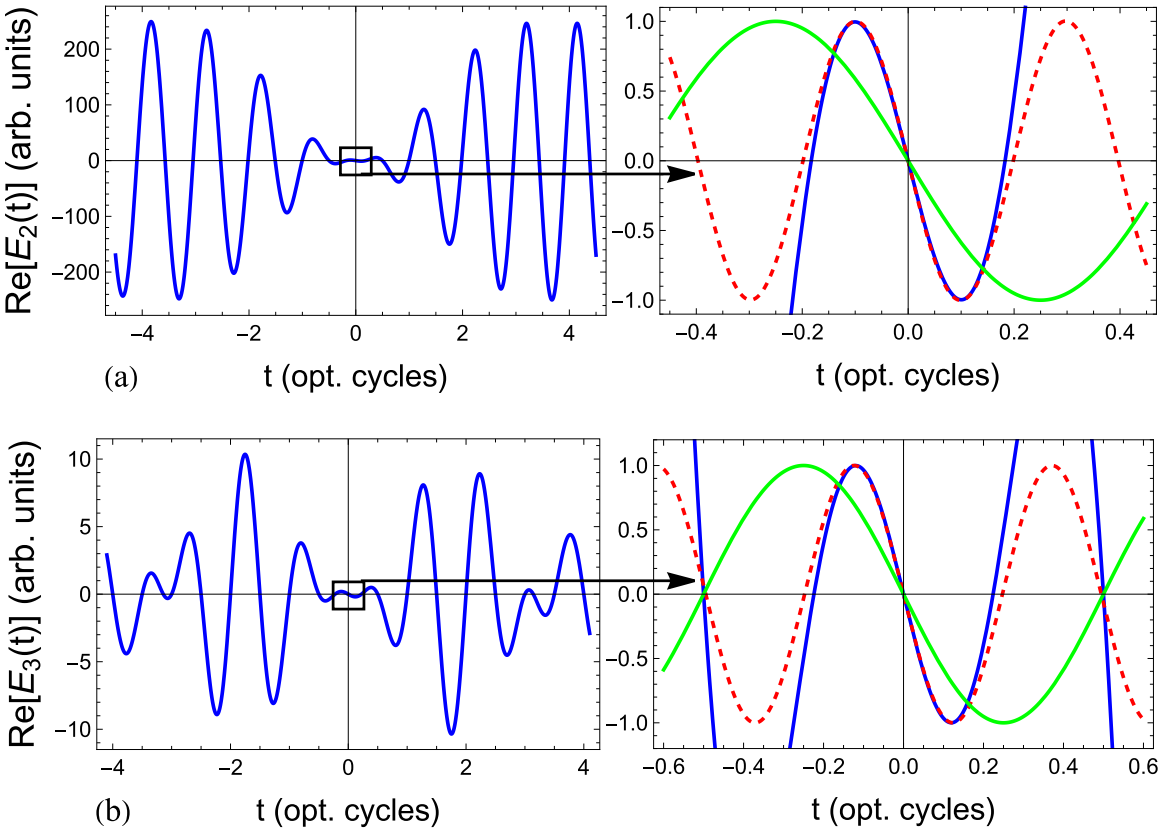

FIG. 2. Comparison between the SO pulses (blue solid lines) $E_2(t)$ (a) and $E_3(t)$ (b), and sine waves at the corresponding frequencies ω_{Pi_Φ} (red dashed lines) and ω_C (green solid lines), respectively. In the left panels, the real part of these fields (Re$[E_i(t)]$, Re$[e^{i\omega_{Pi_\Phi}t}e^{i\frac{\pi}{2}}]$, Re$[e^{i\omega_C t}e^{i\frac{\pi}{2}}]$) are plotted over several optical cycles ($2\pi/\omega_C$) of the sine waves, while in the right panels a zoom over the SO region is depicted.

given by

$$\omega_{P3_\Phi} = \omega_C\left[1+\frac{1}{12}\left(\frac{\Delta\omega_3}{\omega_C}\right)^2\left(\frac{\alpha_3\beta_3^3-1}{\alpha_3\beta_3-1}\right)\right]. \tag{10}$$

Also in this case, when $\alpha_3 \to 0$ we recover the expression for ω_P, i.e., $\omega_{P3_\Phi} \to \omega_{P3} = \omega_C[1+\frac{1}{12}(\frac{\Delta\omega_3}{\omega_C})^2]$,when $\tilde{E}_3(\omega)$ approaches $\tilde{E}_S(\omega)$ [12].

The SO behavior of both pulses, $\tilde{E}_2(\omega)$ and $\tilde{E}_3(\omega)$, becomes clear in the time domain. By Fourier transforming back Eq. (7), we obtain the time-dependent description of $\tilde{E}_2(\omega)$,

$$E_2(t) = \left(e^{-\frac{1}{4}(\Delta\omega_2 t)^2} + \frac{\alpha_2}{\left(1+\beta_2^2\right)^{1/4}}e^{-\frac{1}{4(1+\beta_2^2)}(\Delta\omega_2 t)^2}e^{i\Phi(t)}\right) \times e^{i\omega_C t}e^{i\phi}, \tag{11}$$

with the time-varying phase $\Phi(t) = \frac{\beta_2}{4(1+\beta_2^2)}t^2 - \frac{1}{2}\arctan(\beta_2)+\theta$. Analogously, from Eq. (10), we obtain the time-dependent description of $\tilde{E}_3(\omega)$ as a sum of sinc functions with different temporal widths and amplitudes:

$$E_3(t) = \left[\operatorname{sinc}\left(\frac{\Delta\omega_3 t}{2}\right) - \alpha_3\beta_3\operatorname{sinc}\left(\frac{\beta_3\Delta\omega_3 t}{2}\right)\right]e^{i\omega_C t}e^{i\phi}. \tag{12}$$

Thus, $E_2(t)$ and $E_3(t)$ superoscillate around $t=0$ when the difference between the amplitudes of the interfering fields, i.e., the original pulse that enters the interferometer and the pulse that is broadening in one of its branches, becomes small. This implies that $\frac{\alpha_2}{(1+\beta_2^2)^{1/4}} \to 1$ in the case of $E_2(t)$, and $\alpha_3\beta_3 \to 1$ in the case of $E_3(t)$. In addition, in this central temporal region, the amplitudes of $E_2(t)$ and $E_3(t)$ decrease as $(1-\frac{\alpha_2}{(1+\beta_2^2)^{1/4}})$ and $(1-\alpha_3\beta_3)$, respectively. For example, in the synthesis of $E_3(t)$, if the filtering parameter is chosen as $\beta_3 = 0.5$, the temporal full width at half maximum (FWHM) of the pulse in the SO region approaches zero when $\alpha_3 \to 2$, while $\omega_{P3_\Phi} \to \infty$. As expected, this will be accompanied by a significant reduction in the amplitude of the field: In fact, in that limit, the field amplitude decreases down to zero. A full theoretical description of this phenomenon was done in Ref. [36].

In Fig. 2, we show the real part of $E_2(t)$ and $E_3(t)$ for the set of parameters $\phi = \pi/2$, $\Delta\omega_2 = 1$, $\alpha_2 = 2.24$, $\beta_2 = 5$, and $\Delta\omega_3 = 4$, $\alpha_3 = 1.95$, $\beta_3 = 0.5$, respectively. In these cases, we compare each SO pulse with harmonic waves oscillating at the corresponding frequency ω_{Pi_Φ} (Re$[e^{i\omega_{Pi_\Phi}t}e^{i\phi}]$) and at the central frequency ω_C (Re$[e^{i\omega_C t}e^{i\phi}]$). In particular, because ω_{P2_Φ} results in a complex value, we have plotted Re$[e^{i\mathrm{Re}[\omega_{P2_\Phi}]t}e^{i\phi}]$ instead of Re$[e^{i\omega_{P2_\Phi}t}e^{i\phi}]$. Although we have not yet reached a final conclusion about the physical meaning of Im$[\omega_{P2_\Phi}]$, its value is very small in relation to Re$[\omega_{P2_\Phi}]$ and its effect can be considered, to the first order, negligible. Thus, in the SO region a perfect description of $E_2(t)$ and $E_3(t)$ is obtained through monochromatic fields with frequencies Re$[\omega_{P2_\Phi}]$ and ω_{P3_Φ}, respectively.

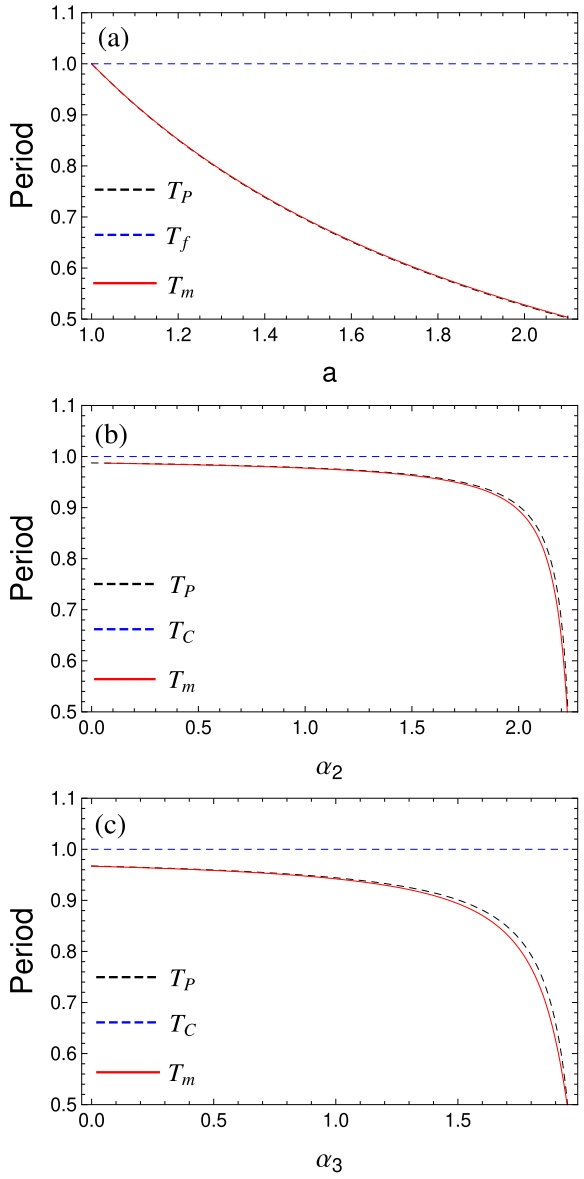

FIG. 3. Comparison between the principal period $T_P \equiv \mathrm{Re}[\frac{2\pi}{\omega_{P_\Phi}}]$ (dashed black lines) and twice the distance between a maximum and its adjacent minimum in the SO region, T_m (red lines), as a function of the SO parameters for (a) $E_1(t)$, (b) $E_2(t)$, and (c) $E_3(t)$. The values are normalized with respect to the period $T_f = \frac{2\pi}{\omega_f}$ in the first case and $T_C = \frac{2\pi}{\omega_C}$ in the other cases.

For a deeper analysis of the use of ω_{P_Φ} in the description of SO pulses, we numerically compare the *principal period*, defined as $T_P = \mathrm{Re}[\frac{2\pi}{\omega_{P_\Phi}}]$, and twice the distance between a maximum and its adjacent minimum in the SO region, T_m. A similar analysis was made in Ref. [12], but considering the original definition of the principal frequency, ω_P, and for a different type of ultrashort pulses in the few-cycle regime, which do not show a SO behavior. In Figs. 3(a)–3(c), we plot the values of T_P (dashed black line) and T_m (red line) for $E_1(t)$, $E_2(t)$, and $E_3(t)$ as a function of the SO parameters, a, α_2, and α_3, respectively. In the first case, the values of T_m and T_P were normalized to $T_f = \frac{2\pi}{\omega_f}$ (dashed blue line) with $\omega_f = 2\pi$, while in the other two cases the normalization is done to the value $T_C = \frac{2\pi}{\omega_C}$ (dashed blue line), with $\omega_C = 2\pi$. The excellent agreement between T_P and T_m, indicates that ω_{P_Φ} is an appropriate value for the frequency that dominates the SO region for the considered fields.

B. Principal frequency of a chirped pulse

In this subsection, we derive the principal frequency $\omega_{P\Phi}$ for a chirped Gaussian pulse with a quadratic phase, also known as group delay dispersion. In the frequency domain, we can write this field as

$$\tilde{E}_\beta(\omega) = e^{-(\frac{\omega-\omega_C}{\Delta\omega})^2} e^{i\beta(\omega-\omega_C)^2}. \tag{13}$$

Equation (13) represents a chirped pulse characterized by a central frequency ω_C, a bandwidth $\Delta\omega$, and the chirp parameter β. Thus, from Eq. (2), we arrive at the following expression:

$$\omega_{P\beta\Phi} = \omega_C\left[1 + \frac{1}{2}\left(\frac{\Delta\omega}{\omega_C}\right)^2\left(\frac{1}{1+\Delta\omega^4\beta^2}\right)\right] - i\,\frac{\Delta\omega^4\beta}{2\omega_C(1+\Delta\omega^4\beta^2)}. \tag{14}$$

The pulse $\tilde{E}_\beta(\omega)$ can be seen as the pulse $\tilde{E}_2(\omega)$ of Eq. (7), when the control parameter α_2 is $\gg 1$. Just like in that case, $\omega_{P\beta\Phi}$ has a nonzero imaginary part and it is necessary to take its real part to characterize the main frequency of the pulse. Furthermore, when the chirp parameter $\beta \to 0$ the imaginary part vanishes and the expression in Eq. (14) converge to the original definition of the principal frequency, ω_P, for a Fourier limited Gaussian pulse, i.e., $\omega_{P\beta_\Phi} \to \omega_C[1 + \frac{1}{2}(\frac{\Delta\omega}{\omega_C})^2]$.

In Fig. 4, we show an example with $\omega_C = 2\pi$ and $\Delta\omega = 2$, which corresponds to a temporal FWHM ≈1.18 optical cycles (FWHM $= 4\frac{\sqrt{\log(2)/2}}{\Delta\omega}$). Figures 4(a)–4(c) correspond to the chirped Gaussian field (blue line) and sine monochromatic fields oscillating at frequency $\mathrm{Re}[\omega_{P\beta\Phi}]$ (red dashed line) and ω_C (green dashed line), respectively. It can be observed the temporal behavior of a Fourier-limited pulse ($\beta = 0$) in Fig. 4(a), a chirped pulse with $\beta = 0.5$ in Fig. 4(b), and a chirped pulse with $\beta = 1$ in Fig. 4(c). Finally, in Fig. 4(d), we show the dependence of the principal frequency normalized to ω_C, i.e., $\mathrm{Re}[\omega_{P\beta\Phi}]/\omega_C$, as a function of the chirp parameter β (blue line). From this figure, it can be seen that $\mathrm{Re}[\omega_{P\beta\Phi}]$ decreases monotonically with β, and converges to the central frequency ω_C when $\Delta\omega^4\beta^2 \gg 1$ [see Eq. (14)]. The last observation agrees with that is expected: For a big enough β, the chirped pulse becomes wider in the time domain and there is no longer an appreciable difference between its central frequency and the principal frequency. Thus, $\omega_{P\beta\Phi} \to \omega_C$ when $\omega_C \gg \Delta\omega$.

C. Optical attosecond pulse

In this subsection, we use the definition of ω_{P_Φ} to analyze an ultrashort pulse covering several octaves in frequency, which has been experimentally synthesized in Refs. [32,33]. Here, the authors were able to synthesize a subcycle pulse in the visible spectrum, called an *optical attosecond pulse*, through a sophisticated experimental setup. A spectral ampli-

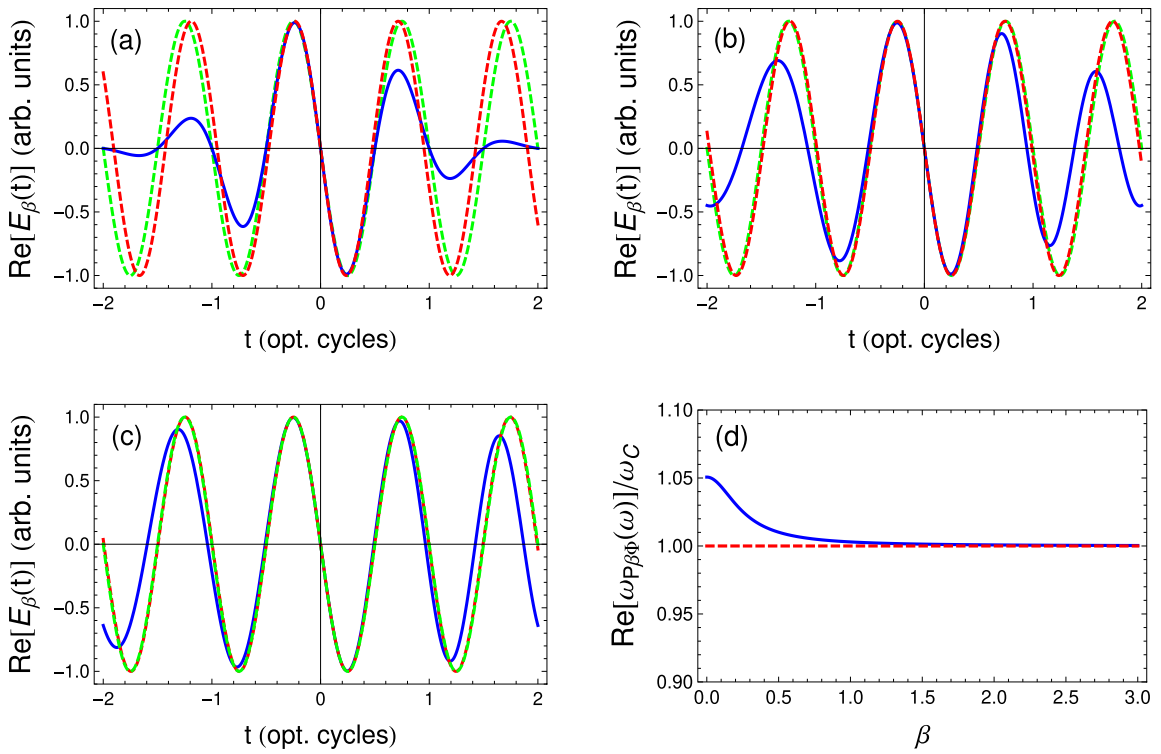

FIG. 4. (a)–(c) Comparison between a Gaussian chirped pulse $E_\beta(t)$ (blue line) and sine waves of frequencies Re$[\omega_{P\beta\Phi}]$ (red dashed line) and ω_C (green dashed line). The values of the chirp parameter β are 0 (a), 0.25 (b), and 1 (c). (d) Evolution of the ratio Re$[\omega_{P\beta\Phi}]/\omega_C$ as a function of β (blue line). The value of ω_C was normalized to the unity (red dashed line).

tude $|\tilde{E}_4(\omega)|$, similar to that of such a pulse, can be seen in Fig. 5(a). For this case, the spectral phase $\Phi(\omega)$ is constant, so we have numerically obtained the value of the principal frequency directly from $|\tilde{E}_4(\omega)|$. This was done through a polynomial interpolation of the spectrum $|\tilde{E}_4(\omega)|$ to subsequently calculate the integrals in Eq. (2). In arbitrary units, we have obtained that $\omega_{P4_\Phi} = 4.23$ (black line), while the value of its carrier frequency, obtained similarly from its definition [34], is $\omega_0 = 3.2$ in arbitrary units (orange line).

The optical attosecond pulse in the time domain $E_4(t)$ is shown in Fig. 5(b) for both a sinelike global phase (blue line, $\phi = \pi/2$) and a cosinelike global phase (red line, $\phi = 0$). We also show a monochromatic field oscillating at frequency ω_{P4_Φ}, with a cosinelike global phase (dashed green line) and with a sinelike global phase (dashed black line). In the central region, it can be seen that ω_{P4_Φ} allows us to describe the position of the peak values of the field in both cases as well as the general shape of the pulse with $\phi = \pi/2$ before the first zero crossing.

As mentioned in Sec. II, one of the main motivations for extending the original definition of the principal frequency ω_P [Eq. (1)] was to include the spectral phase $\Phi(\omega)$ of the field, which is relevant to describe, for example, SO pulses. For the attosecond optical pulse, however, since $\Phi(\omega)$ is constant, it does not play any role in the expression of ω_{P_Φ} [Eq. (2)]. Even so, ω_{P4_Φ} differs from the value of the principal frequency ω_P. In fact, in arbitrary units, we have obtained a value $\omega_P = 3.63$, which represents a shift of $\approx$17%, toward lower frequencies with respect to ω_{P4_Φ}. This difference arises from the fact that this extended definition of the principal frequency is weighted by the field $\tilde{E}(\omega) = |\tilde{E}(\omega)|e^{i\Phi(\omega)}$ instead of the spectral power $S(\omega)$, which allows us to represent, in a much better way, the main frequency of ultrashort pulses with complex spectral content, with and without a particular spectral phase. Only when the spectral content of the pulse is symmetric (and $\Phi(\omega)$ is constant), as is the case for Gaussian or sinc pulses, the values of ω_P and ω_{P_Φ} are equal.

III. PRINCIPAL FREQUENCY, SUPER-BANDWIDTH, AND LHG

In this section, we analyze the nonlinear interaction between an atomic system and a SO pulse like the one given by Eq. (12). For that purpose, after computing the LHG spectrum, we appeal to both the definition of ω_{P_Φ} and the effective superbandwidth of the pulse to characterize the generated harmonics.

As a first step, we calculate the dipole acceleration $a(t)$ quantum mechanically. $a(t)$ was obtained through the numerical integration of the 1D-TDSE in a hydrogen atom (for more details see, e.g., Ref. [38]). After that, a time-frequency (wavelet) analysis has been performed to extract temporal information from the LHG spectrum. Here, we employ the Gabor transform to obtain $a_G(\Omega, t)$, defined as

$$a_G(\Omega, t) = \int dt' a(t') \frac{\exp[-(t-t')^2/2\sigma^2]}{\sigma\sqrt{2\pi}} \exp(i\Omega t'), \quad (15)$$

where the integration is usually taken over the pulse duration, and σ is chosen in such a way that a suitable balance between the time and frequency resolutions is achieved. In our case,

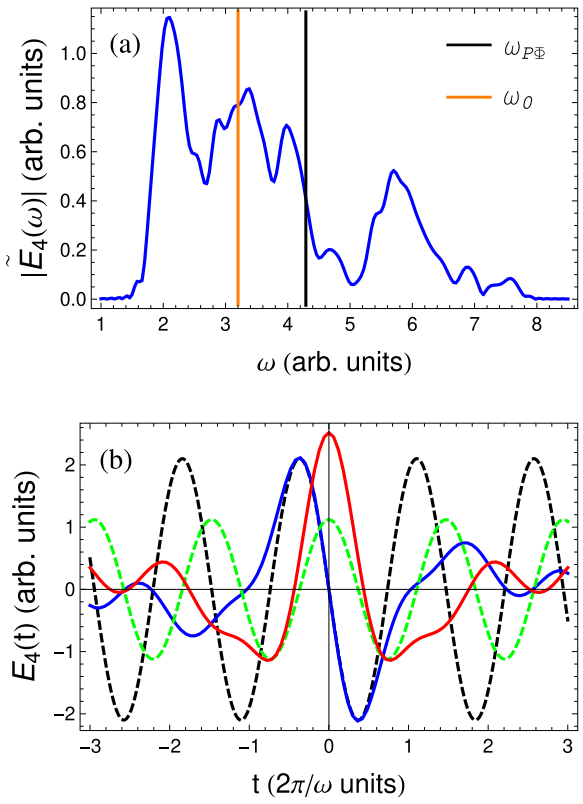

FIG. 5. (a) Spectral amplitude $|\tilde{E}_4(\omega)|$ of the optical attosecond pulse. (b) Temporal profile $E_4(t)$, with a cosinelike global phase (red line) and a sinelike global phase (blue line). Monochromatic fields oscillating at the frequency ω_{P4_Φ} are plotted for a cosinelike (dashed green line) and a sinelike (dashed black line) phase.

we have used $\sigma = 4/\omega_C$ for an appropriate resolution of the LHG spectrum.

Numerical results

To perform our simulations, we consider, as a driving field, the SO pulse $E_3(t)$ defined in Sec. II A, with a central wavelength of $\lambda_C = 1200$ nm and a peak intensity $I_0 = 5 \times 10^{13}$ W/cm^2 in the SO region. The bandwidth, in units of $\omega_C = 2\pi$, is set to $\Delta\omega_3 = 4$, and the values of the synthesis parameters are chosen to be $\beta_3 = 0.5$, while α_3 is varied ($\alpha_3 = 0, 0.6, 1$). It should be noted that for $\alpha_3 = 0$ we have a sinclike pulse [Eq. (12)], thus the temporal FWHM is $\approx 5.564/\Delta\omega_3$ (see Ref. [12]), which in the present example corresponds to 1.4 optical cycles. For $\alpha_3 = 0.6$ and $\alpha_3 = 1$, the value of FWHM in the SO region is reduced to 1.2 and 1 optical cycles, respectively.

In Fig. 6, we show plots of $|a_G(\Omega, t)|^2$ (in log scale) for the different studied cases. The dependence on t is expressed in opt. cycles (optical cycles), while the dependence on the frequency Ω is derived from the order of the harmonic. The corresponding driving field $E_3(t)$ is overlapped to show the evolution of the radiation emission with the pulse duration. We observe that the third and fifth harmonics are emitted in the temporal region corresponding to the central region of the pulse (the SO region), with an efficiency that decreases with the harmonic order. The fundamental harmonic, which lies in the saturated region in the lower part of the plots, has an intensity that is seven orders of magnitude greater than those of the third and fifth harmonics. For $\alpha_3 = 0.6$ and $\alpha_3 = 1$, the radiation is emitted as harmonics in the temporal regions corresponding to the side lobes of the pulse as well, which is typical of the SO phenomenon. Indeed, the interference fringes can be understood as a consequence of the coherent superposition between the harmonic radiation generated by the SO region and that generated by the respective side lobes.

For a better visualization of the evolution of the fundamental, third, and fifth harmonics as a function of the synthesis parameter α_3, we show in Fig. 7, a cross section of the contour plots in the SO region (corresponding to the dashed white line in Fig. 6). We present both the sinelike (continue lines) and cosinelike (dashed lines) phases. Two relevant phenomena can be extracted from this figure.

(i) There is a broadening of the harmonics bandwidth as α_3 increases. For the fundamental harmonic, this result is equivalent to the one observed in Ref. [29]. This spectral broadening is quantified by the horizontal arrows in Fig. 7, indicating the FWHM of the harmonics. For the fundamental harmonic the FWHM is approximately 1.12 and 1.39 for $\alpha_3 = 0.6$ and $\alpha_3 = 1$, respectively (here a FWHM equal to 1 corresponds to the FWHM of the driving field, i.e., when $\alpha_3 = 0$). In the case of the third harmonic, we have a broadening of 1.11 (for $\alpha_3 = 0.6$) and 1.2 (for $\alpha_3 = 1$), and for the fifth harmonic this broadening is 1.09 (for $\alpha_3 = 0.6$) and 1.19 (for $\alpha_3 = 1$).

(ii) A blueshift can be seen in the peak positions of the third and fifth harmonics, for all values of α_3. Furthermore, this shift increases with α_3. For the fundamental harmonic, however, this phenomenon is not observed. To quantify this shift, we compute the principal frequency ω_{P3_Φ} for each set of values of the synthesis parameters $\{\Delta\omega_3 = 4, \beta_3 = 0.5, \alpha_3 = 0, 0.6, 1\}$, and calculated the third and fifth harmonics as $3\frac{\omega_{P3_\Phi}}{\omega_C}$ and $5\frac{\omega_{P3_\Phi}}{\omega_C}$, respectively. We have obtained that $3\frac{\omega_{P3_\Phi}}{\omega_C} \approx 3.10, 3.14, 3.18$, while $5\frac{\omega_{P3_\Phi}}{\omega_C} \approx 5.17, 5.22, 5.30$, in order of increasing α_3. These values are represented by the vertical colored lines in Fig. 7, and it is clearly seen that they coincide with the central frequency of the respective harmonic order.

Finally, it should be noted that the spectral characteristics of the LHG for different global phases ϕ (sinelike and cosinelike) of the driving pulse show that only noticeable changes are observed in the fifth harmonic. For $\alpha_3 = 0$ and $\alpha_3 = 0.6$, a slight broadening can be seen in the spectrum for the cosinelike (dashed line) phase, in relation with the sinelike one, while for $\alpha_3 = 1$ the spectrum broadens toward a continuum (dashed green line). These results are in agreement with the nonlinear response of bound electrons studied with subcycle pulses [33].

IV. DISCUSSION

Here we discuss the physical implications and the consequences of the results presented in Sec. III. We also put forward some questions that naturally remain open, since they need a deeper analysis beyond the possible practical applications and the scope of the present paper.

First, the introduction of the principal frequency ω_P turns out to be instrumental to identify the frequency that dominates the interaction between an ultrashort pulse and matter,

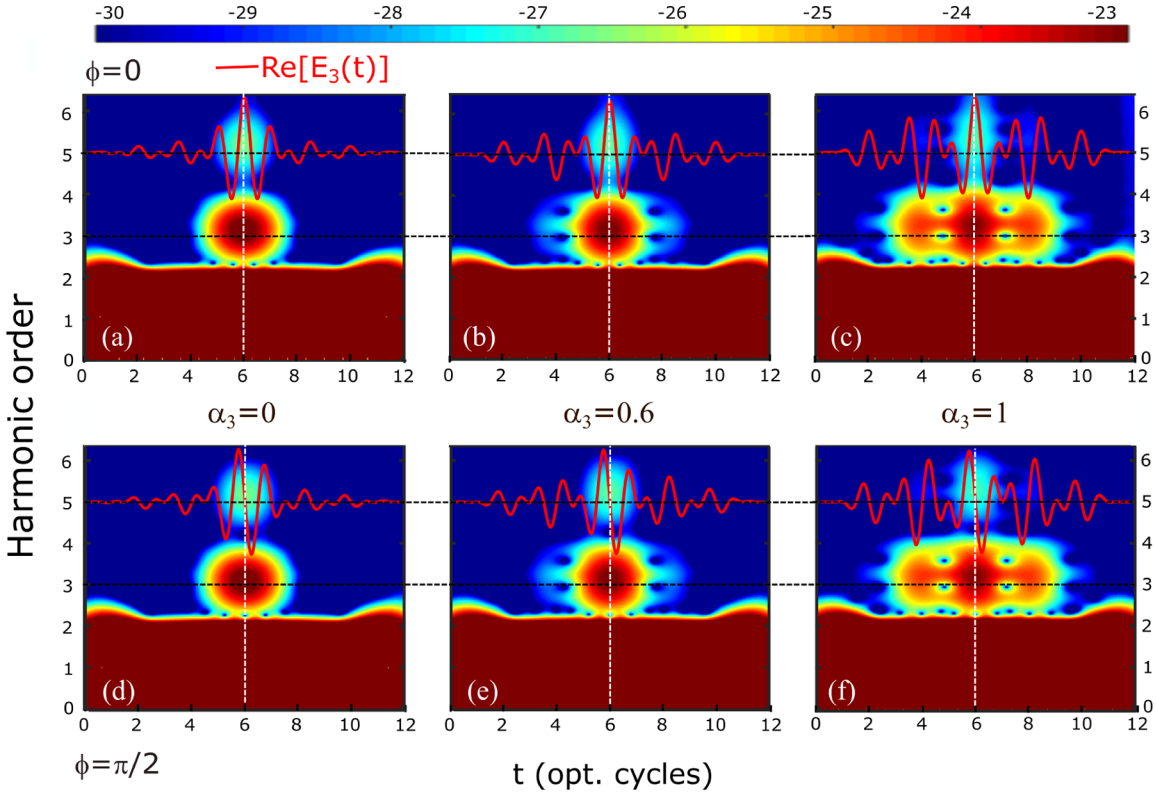

FIG. 6. Contour plot of $|a_G(\Omega, t)|^2$ (in log scale) as a function of time and harmonic order for different values of the synthesis parameter α_3, related to the SO behavior of the driving field $E_3(t)$. From plots (a)–(c), we set the global phase of $E_3(t)$ to be $\phi = 0$ while from plots (d)–(f) it is $\phi = \pi/2$. The values of α_3 are indicated between the top and bottom panels. The corresponding synthesized pulse $E_3(t)$, used as driving field for the simulations, is included in each panel (red line), expressed in arbitrary units.

in the nonlinear regime, as well as being the key parameter in describing the main frequency of SO pulses. Previously, in Ref. [12], we studied the HHG in atoms. In that work, we showed that the more energetic photon that is generated (cutoff) is better predicted by ω_P instead of ω_0. In addition, the extended version of ω_P introduced in the present paper, and which we refer to as ω_{P_Φ}, allows, on the one side, a very good description of the main frequency of ultrashort pulses with complex spectral content like the *optical attosecond pulse*. On the other side, since this extended definition incorporates the spectral phase $\Phi(\omega)$, a good description of the SO frequency is obtained. In this regard, we have shown that a monochromatic field with frequency $\omega_{P\Phi}$ satisfactorily describes the respective time-dependent SO field and we have presented a mathematical expression to quantify the SO frequency.

In relation to the blueshift of the central peak of the LHG observed in the present paper, we can introduce the following analysis: In perturbation theory, the nonlinear polarization $P_{\rm NL}(t)$, for an instantaneous response and a centrosymmetric medium, relates to the driving field $E(t) = A(t)e^{i\omega_C t}$ as $P_{\rm NL}(t) = \chi_3 E(t)^3 + \chi_5 E(t)^5$, where the parameters χ_3 and χ_5 are the electrical nonlinear susceptibilities (we consider

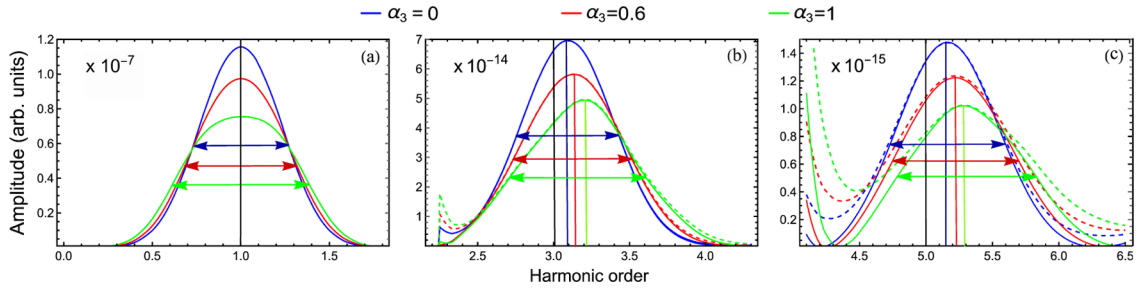

FIG. 7. Spectrum of the fundamental (a), third (b), and fifth (c) harmonic obtained from a vertical cut, in the SO region, of the contour plots of Fig. 6 (see there the white dashed lines). Each color indicates a different value of the synthesis parameter α_3. Continuous lines (dashed lines) correspond to a driving field $E_3(t)$ with a global phase $\phi = \frac{\pi}{2}$ ($\phi = 0$). Vertical color lines indicate the central frequency of the harmonics as quantified by the principal frequency $\omega_{P3_\Phi}(\alpha_3)$ as $3\frac{\omega_{P3_\Phi}(\alpha_3)}{\omega_C}$ and $5\frac{\omega_{P3_\Phi}(\alpha_3)}{\omega_C}$, for the third and fifth harmonics, respectively. For comparison, black vertical lines indicate the central frequency of the third and fifth harmonics as quantified by $3\omega_C$ and $5\omega_C$, respectively, being ω_C the central frequency of the driving field. Horizontal arrows indicate the temporal FWHM of the corresponding harmonic.

here up to fifth order). This implies that the harmonic fields $E_3(t)$ and $E_5(t)$ can be written as $E_3(t) = A_3(t)e^{i\omega_{C3}t}$ and $E_5(t) = A_5(t)e^{i\omega_{C5}t}$, with $A_3(t)$ and $A_5(t)$ the fields envelopes, and central frequency $\omega_{C3} = 3\omega_C$ and $\omega_{C5} = 5\omega_C$, respectively. However, our results show that the central frequencies of the harmonics are $\omega_{C3} = 3\omega_{P_\Phi}(\Delta\omega, \omega_C)$ and $\omega_{C5} = 5\omega_{P_\Phi}(\Delta\omega, \omega_C)$, i.e., they are not only dependent on the central frequency of the driving field ω_C but also on its bandwidth $\Delta\omega$. These results are equivalent to those presented in Ref. [39], where the blueshift is originated by a photon acceleration phenomenon, which could be related with the properties of the nonlinear medium. In our case, on the contrary, the blueshift is given by the principal frequency that is a characteristic of the laser pulse itself and is, therefore, independent of the medium. This fact would allow us to apply the principal frequency concept in other nonlinear processes, for instance, the above-threshold ionization in atoms [40] or HHG in solids [41], just to name a few.

The original idea behind the introduction of the principal frequency was to give a higher weight to the more energetic frequencies (or photons) in the density distribution $\rho_P(\omega) = \omega S(\omega)$. The extended version of the density distribution $\rho_{P_\Phi}(\omega) = \omega|\tilde{E}(\omega)|e^{i\Phi(\omega)}$ is a complex-valued function that also gives a higher weight to the more energetic photons, but now it takes into account the spectral phase of the field. A question that arises is, What is the real physical meaning of the complex-valued principal frequency? In the temporal domain, the distribution $\rho_{P_\Phi}(\omega)$ is the derivative of the field $\frac{dE(t)}{dt}$ that can be obtained using Fourier transform properties. Therefore, is there a relation between $P_{\rm NL}(t)$ and $\frac{dE(t)}{dt}$?

Second, beyond the concept of the principal frequency, the most relevant result presented in this paper is the possibility to generate *new frequencies or photons* in a laser pulse through a linear synthesis, lacking the need of a material medium. Although the concept of *superbandwidth* in laser pulses was presented in Ref. [29] through the analysis of the stationary points in a two-level system, the study done in the present paper is much more powerful and universal. This is because we have used *ab initio* tools, the solution of the 1D-TDSE, and the analysis of the emitted radiation by a wavelet transform. Moreover, the *superbandwidth* appears here as a broadening of the bandwidth of the studied harmonics and is in excellent agreement with the value extracted from the dependence of the principal frequency ω_{P_Φ} with the bandwidth.

One of the questions that can be gleaned from the previous paragraph is, Which is the limit for the *new frequencies or photons* that can be generated by this interferometric method? A similar question—*How can an infrared photon behave as a gamma ray?*—was analyzed in Ref. [42]. Theoretically, it seems that there is not such a limit but, experimentally, an extremely precise control of the phase between the interferometer arms is necessary to maintain the condition of destructive interference. In addition, for a fixed value of the filtering parameter β_3, it is necessary, as well, to have precise control of the relative field amplitudes between the interferometer arms, α_3.

Finally, what happens with the global phase ϕ, in the SO region, when $\omega_P \gg \omega_C$ (i.e., the temporal FWHM $\to 0$)? In the SO region, are there changes in the spectral properties of the pulse when ϕ varies in that limit?

V. CONCLUSIONS

In this paper, we have extended the definition of the principal frequency by changing the *weight* function in the spectral power $S(\omega)$ of a field $\tilde{E}(\omega)$, now including its spectral phase $\Phi(\omega)$. We show that, for the SO pulses presented as examples, this redefinition gives a frequency value that allows a good description of the main frequency in the SO region. In addition, we have demonstrated that the principal frequency describes the main frequency of an optical attosecond pulse, with a very complex spectral content. We can conclude that the concept of principal frequency can be more suitable in the characterization of the main frequency of pulses emerging from complex synthesis techniques instead of the conventional central frequency (wavelength), which is the standard experimental parameter used for that purpose (see, for example, Refs. [32,33,43–45]).

Simultaneously, we have analyzed the nonlinear interaction properties of SO pulses, in the few-cycle regime, with a hydrogen atomic system, by solving the 1D-TDSE. Particularly, we studied the fundamental, third, and fifth harmonics through a wavelet analysis, and showed that their spectral characteristics are well described by resorting to the principal frequency and the effective superbandwidth of the pump pulse. Finally, we made a discussion of the physical implications of our results, while some questions remain open.

The possibility to manipulate the spectral and temporal characteristics of a pulse in the SO region could be of great interest for a wide variety of applications, ranging from coherent control to femto/attosecond spectroscopy. On the other hand, the broadening of the fundamental harmonic as a *superbandwidth* clearly shows that pulses in the SO region interact, in the weak field regime, as if they would have new frequencies or photon energies, i.e., new frequencies are being generated through a linear synthesis. In the same way that the SO phenomenon is a wave phenomenon, this analysis can be extended to all kind of signals as, e.g., acoustic waves, coherent sources, matter waves, etc.

The case of a chirped pulse analyzed in Sec. II B could indeed have practical applications. As shown, the extended definition of the principal frequency depends on the chirp parameter β. As a consequence, we can envision the possibility to experimentally characterize Fourier-limited pulses in the few-cycle, single-cycle, and subcycle regimes. In fact, when the value of the chirp parameter approaches zero, the principal frequency reaches a maximum. Therefore, by looking for the central position of the third or fifth harmonics, it should be possible to determine if the pulse has a spectral phase (chirp), i.e., if the blueshift of the harmonics is maximum when the pulse is Fourier limited.

Another attractive arena where the extended definition of the principal frequency might be relevant is the interaction of strong laser pulses with solid materials. Here, it was demonstrated that coherent radiation in the extreme XUV range can be generated by driven bulk samples with subcycle pulses [32]. A correct characterization of this generated radiation could indeed be performed using the extended definition of the principal frequency. Another area of research would be to use SO pulses to drive solid samples. For this case, for instance, we expect the role of the intra- and interband dynamics to

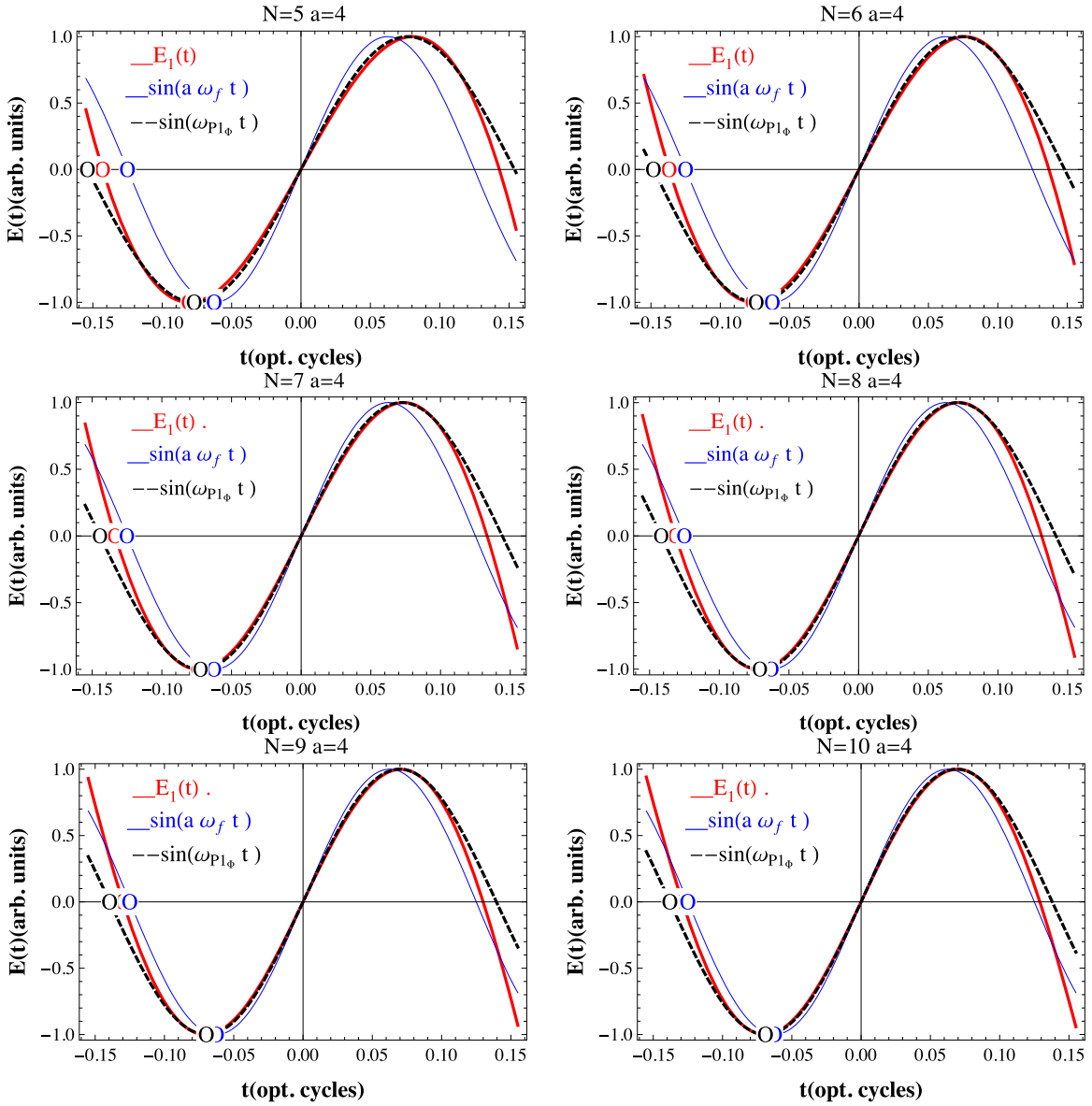

FIG. 8. Comparison between zero crossing points and minima of the real part of the SO function $E_1(t)$ (red solid lines) and sine waves at the frequencies ω_{P1_Φ} (dashed black lines) and $\omega_{SO} = a\omega_f$ (solid blue lines). The superoscillatory degree, accounted for by the parameter a, is held at 4 for all curves, while N varies from 5 to 10. It can be seen that the difference between $\mathrm{Re}[E_1(t)]$ and $\mathrm{Re}[e^{ia\omega_f t}e^{i\frac{\pi}{2}}] = \sin(a\omega_f t)$ is larger than that with respect to $\mathrm{Re}[e^{i\omega_{P1_\Phi} t}e^{i\frac{\pi}{2}}] = \sin(\omega_{P1_\Phi} t)$.

be different compared with the case of conventional laser pulses. The extended definition of the principal frequency could shed light about the underlying physics of these strong field processes. Finally, we envision the introduction of the principal frequency could generate great interest in strong field processes driven by field transients [46] and asymmetric single-cycle pulses [7].

ACKNOWLEDGMENTS

M.F.C. acknowledges financial support from the Guangdong Province Science and Technology Major Project (Future functional materials under extreme conditions - 2021B0301030005). E.G.N. acknowledges Consejo Nacional de Investigaciones Científicas y Técnicas (CONICET). F.V. acknowledges Comisión de Investigaciones Científicas de la Pcia. de Buenos Aires.

APPENDIX: PRINCIPAL FREQUENCY AND DEGREE OF FITTING WITH SO FUNCTIONS

We present here a numerical analysis of the SO frequency for the field $E_1(t)$ [Eq. (3)], at a fixed value of the SO parameter a (also called degree of superoscillation [21]), while varying the value of N. For each pair of values $\{N, a\}$, we compare the degree of fitting in the description of the peaks' values (maxima and minima) and zero crossing points of the field $E_1(t)$, when the principal frequency, ω_{P1_Φ}, or the conven-

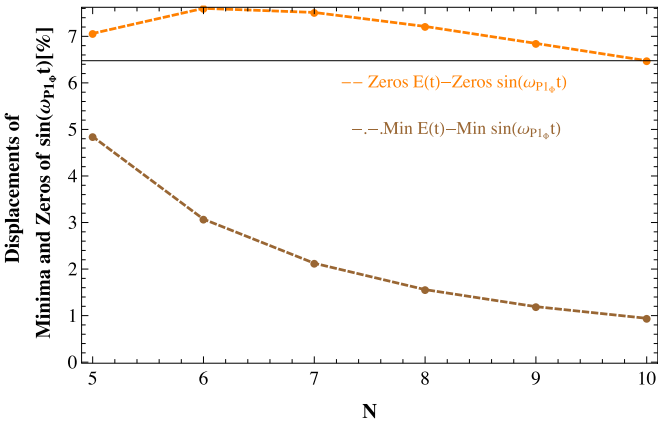

FIG. 9. Difference between the minima (brown dashed-dot lines) and zeros (orange dashed lines) of Re$[E_1(t)]$ and those extracted from Re$[e^{i\omega_{P1_\Phi}t}e^{i\frac{\pi}{2}}] = \sin(\omega_{P1_\Phi}t)$. These differences correspond to the curves shown in Fig. 8, where $a = 4$ for all values of N.

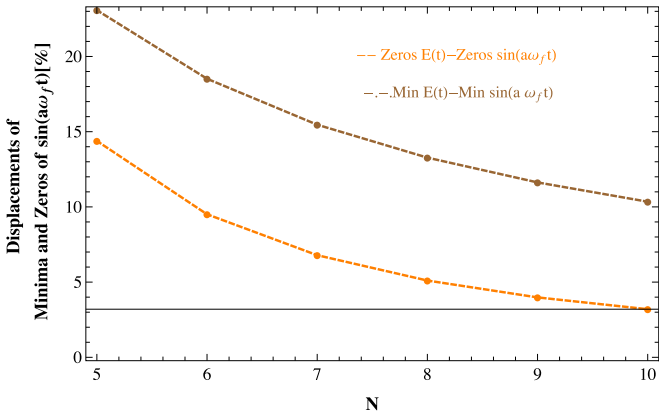

FIG. 10. Difference between the minima (brown dashed-dot lines) and zeros (orange dashed lines) of Re$[E_1(t)]$ and those of Re$[e^{ia\omega_f t}e^{i\frac{\pi}{2}}] = \sin(a\omega_f t)$. These differences correspond to the curves shown in Fig. 8, where $a = 4$ for all values of N.

tional SO frequency, $\omega_{SO} = a\omega_f$, are used. For that purpose, the real part of the field $E_1(t)$, with a global phase $\phi = \pi/2$, is compared against sinusoidal signals with frequencies ω_{P1_Φ} and ω_{SO}.

Figure 8 depicts the curves of interest, Re$[E_1(t)]$, Re$[e^{i\omega_{P1_\Phi}t}e^{i\phi}]$, and Re$[e^{ia\omega_f t}e^{i\phi}]$, when $a = 4$, and N ranges from $N = 5$ to $N = 10$. The time axis is displayed in units of optical cycles, normalized to $2\pi/\omega_f$, in a range that allows summarizing the main features of the fields in the SO region (it is the range where the first extreme values of the curves are localized). The analysis is done on the positions of zeros and minima of the different curves (color circles), but the same conclusions could be obtained by analyzing the maxima, since maxima and minima, as well as the zero crossings, are localized symmetrically to $t = 0$ (the minima in the interval $[-0.10, -0.05]$, the maxima in the interval [0.05,0.10]). From these plots, it can be observed that the agreement between Re$[E_1(t)]$ (solid red lines) and Re$[e^{i\omega_{P1_\Phi}t}e^{i\phi}]$ (black dashed lines) is better than that with Re$[e^{ia\omega_f t}e^{i\phi}]$ (solid blue lines), considering the interval between the minimum and its adjacent maximum. We note, however, the latter field represents better the zero crossing points of Re$[E_1(t)]$. Besides, the fitting using both $a\omega_f$ and ω_{P1_Φ} improves as N increases. Although we show here the analysis for a single value of the parameter a, this behavior is universal.

From the results of Fig. 8, we plot, in Fig. 9, the difference between the zeros (orange dashed lines) and minima (brown dot-dashed lines) of $E_1(t)$ and those of Re$[e^{i\omega_{P1_\Phi}t}e^{i\phi}]$, when N varies. Additionally, and for comparison purposes, we show in Fig. 10 the curves corresponding to the difference between the zeros (orange dashed lines) and minima (brown dot-dashed lines) between $E_1(t)$ and Re$[e^{ia\omega_f t}e^{i\phi}]$ as a function of N. In the first case (Fig. 9), the difference between the zeros remains around 7% (orange dashed line) for all N, while for the minima we observe a decrease from 5 to 1 % (brown dashed line) as N increases. These differences, for both the zeros and minima, are considerably smaller than those between $E_1(t)$ and a sine wave at the SO frequency $a\omega_f$, Re$[e^{ia\omega_f t}e^{i\phi}]$ (see Fig. 10). In the last case, the difference between zeros ranges from 15% to 3%, while for the minima it is ranges from 23% to 10%.

Finally, it must be mentioned that an analytical demonstration can be followed to show the convergence of ω_{SO} to $a\omega_f$, when $N \to \infty$ [20]. Moreover, we have shown in Sec. II A that $\omega_{P1_\Phi} = a\omega_f$ in such a limit ($N \to \infty$). Beyond these analytical results, we show here that, for $N > 1$ but finite, and for the first extreme values of the SO function $E_1(t)$, a sine wave at ω_{P1_Φ} is a better fit than a sine wave at $a\omega_f$. This can be particularly recognized in Fig. 8, especially for the smallest values of N.

[1] T. Brabec and F. Krausz, Intense few-cycle laser fields: Frontiers of nonlinear optics, Rev. Mod. Phys. **72**, 545 (2000).

[2] G.-Q. Liao, H. Liu, G. G. Scott, Y.-H. Zhang, B.-J. Zhu, Z. Zhang, Y.-T. Li, C. Armstrong, E. Zemaityte, P. Bradford *et al.*, Towards Terawatt-Scale Spectrally Tunable Terahertz Pulses Via Relativistic Laser-Foil Interactions, Phys. Rev. X **10**, 031062 (2020).

[3] C. Manzoni, O. D. Mücke, G. Cirmi, S. Fang, J. Moses, S.-W. Huang, K.-H. Hong, G. Cerullo, and F. X. Kärtner, Coherent pulse synthesis: Towards sub-cycle optical waveforms, Laser Photonics Rev. **9**, 129 (2015).

[4] S. Haessler, T. Balciunas, G. Fan, G. Andriukaitis, A. Pugzlys, A. Baltuska, T. Witting, R. Squibb, A. Zair, J. W. G. Tisch, J. P. Marangos, and L. E. Chipperfield, Optimization of Quantum Trajectories Driven by Strong-Field Waveforms, Phys. Rev. X **4**, 021028 (2014).

[5] F. Krausz and M. I. Stockman, Attosecond metrology: From electron capture to future signal processing, Nat. Photonics **8**, 205 (2014).

[6] T. Rybka, M. Ludwig, M. F. Schmalz, V. Knittel, D. Brida, and A. Leitenstorfer, Sub-cycle optical phase control of nanotunnelling in the single-electron regime, Nat. Photonics **10**, 667 (2016).

[7] Y. Morimoto, Y. Shinohara, M. Tani, B.-H. Chen, K. L. Ishikawa, and P. Baum, Asymmetric single-cycle control of valence electron motion in polar chemical bonds, Optica **8**, 382 (2021).

[8] P. Corkum and F. Krausz, Attosecond science, Nat. Phys. **3**, 381 (2007).

[9] F. Calegari, G. Sansone, S. Stagira, C. Vozzi, and M. Nisoli, Advances in attosecond science, J. Phys. B: At. Mol. Opt. Phys. **49**, 062001 (2016).

[10] K. Amini, J. Biegert, F. Calegari, A. Chacón, M. F. Ciappina, A. Dauphin, D. K. Efimov, C. F. de Morisson Faria, K. Giergiel, P. Gniewek *et al.*, Symphony on strong field approximation, Rep. Prog. Phys. **82**, 116001 (2019).

[11] F. Krausz and M. Ivanov, Attosecond physics, Rev. Mod. Phys. **81**, 163 (2009).

[12] E. G. Neyra, P. Vaveliuk, E. Pisanty, A. S. Maxwell, M. Lewenstein, and M. F. Ciappina, Principal frequency of an ultrashort laser pulse, Phys. Rev. A **103**, 053124 (2021).

[13] M. Chini, X. Wang, Y. Cheng, H. Wang, Y. Wu, E. Cunningham, P.-C. Li, J. Heslar, D. A. Telnov, S.-I. Chu *et al.*, Coherent phase-matched VUV generation by field-controlled bound states, Nat. Photonics **8**, 437 (2014).

[14] D. C. Yost, T. R. Schibli, J. Ye, J. L. Tate, J. Hostetter, M. B. Gaarde, and K. J. Schafer, Vacuum-ultraviolet frequency combs from below-threshold harmonics, Nat. Phys. **5**, 815 (2009).

[15] A. Spott, A. Jaroń-Becker, and A. Becker, Ab initio and perturbative calculations of the electric susceptibility of atomic hydrogen, Phys. Rev. A **90**, 013426 (2014).

[16] A. Spott, A. Becker, and A. Jaroń-Becker, Transition from perturbative to nonperturbative interaction in low-order-harmonic generation, Phys. Rev. A **91**, 023402 (2015).

[17] M. Lewenstein, P. Balcou, M. Y. Ivanov, A. L'Huillier, and P. B. Corkum, Theory of high-harmonic generation by low-frequency laser fields, Phys. Rev. A **49**, 2117 (1994).

[18] W.-H. Xiong, J.-W. Geng, J.-Y. Tang, L.-Y. Peng, and Q. Gong, Mechanisms of Below-Threshold Harmonic Generation in Atoms, Phys. Rev. Lett. **112**, 233001 (2014).

[19] W.-H. Xiong, L.-Y. Peng, and Q. Gong, Recent progress of below-threshold harmonic generation, J. Phys. B: At. Mol. Opt. Phys. **50**, 032001 (2017).

[20] Y. Aharonov, F. Colombo, I. Sabadini, D. Struppa, and J. Tollaksen, *The Mathematics of Superoscillations* (American Mathematical Society, Rhode Island, 2017).

[21] M. V. Berry and S. Popescu, Evolution of quantum superoscillations and optical superresolution without evanescent waves, J. Phys. A: Math. Gen. **39**, 6965 (2006).

[22] M. Berry, N. Zheludev, Y. Aharonov, F. Colombo, I. Sabadini, D. C. Struppa, J. Tollaksen, E. T. F. Rogers, F. Qin, M. Hong, X. Luo, R. Remez, A. Arie, J. B. Götte, M. R. Dennis, A. M. H. Wong, G. V. Eleftheriades, Y. Eliezer, A. Bahabad, G. Chen *et al.*, Roadmap on superoscillations, J. Opt. **21**, 053002 (2019).

[23] S. Zarkovsky, Y. Ben-Ezra, and M. Schwartz, Transmission of superoscillations, Sci. Rep. **10**, 5893 (2020).

[24] G. Chen, Z.-Q. Wen, and C.-W. Qiu, Superoscillation: From physics to optical applications, Light Sci. Appl. **8**, 56 (2019).

[25] K. S. Rogers and E. T. F. Rogers, Realising superoscillations: A review of mathematical tools and their application, J. Phys. Photonics **2**, 042004 (2020).

[26] F. Colombo, I. Sabadini, D. C. Struppa, and A. Yger, Superoscillating sequences and supershifts for families of generalized functions, Complex Anal. Oper. Theory **16**, 34 (2022).

[27] S. Brehm, A. V. Akimov, R. P. Campion, and A. J. Kent, Temporal superoscillations of subterahertz coherent acoustic phonons, Phys. Rev. Res. **2**, 023009 (2020).

[28] R. Ber, O. Kenneth, and B. Reznik, Superoscillations underlying remote state preparation for relativistic fields, Phys. Rev. A **91**, 052312 (2015).

[29] E. G. Neyra, D. A. Biasetti, P. Vaveliuk, G. A. Torchia, M. F. Ciappina, F. Videla, and L. Rebón, Effective super-bandwidth in laser pulses, Opt. Lett. **46**, 4761 (2021).

[30] Y.-M. He, H. Wang, C. Wang, M.-C. Chen, X. Ding, J. Qin, Z.-C. Duan, S. Chen, J.-P. Li, R.-Z. Liu *et al.*, Coherently driving a single quantum two-level system with dichromatic laser pulses, Nat. Phys. **15**, 941 (2019).

[31] Z. X. Koong, E. Scerri, M. Rambach, M. Cygorek, M. Brotons-Gisbert, R. Picard, Y. Ma, S. I. Park, J. D. Song, E. M. Gauger, and B. D. Gerardot, Coherent Dynamics in Quantum Emitters Under Dichromatic Excitation, Phys. Rev. Lett. **126**, 047403 (2021).

[32] T. T. Luu, M. Garg, S. Y. Kruchinin, A. Moulet, M. T. Hassan, and E. Goulielmakis, Extreme ultraviolet high-harmonic spectroscopy of solids, Nature (London) **521**, 498 (2015).

[33] M. T. Hassan, T. T. Luu, A. Moulet, O. Raskazovskaya, P. Zhokhov, M. Garg, N. Karpowicz, A. Zheltikov, V. Pervak, F. Krausz *et al.*, Optical attosecond pulses and tracking the nonlinear response of bound electrons, Nature (London) **530**, 66 (2016).

[34] J.-C. Diels and W. Rudolph, *Ultrashort Laser Pulse Phenomena Fundamentals, Techniques, and Applications an a Femtosecond Time Scale*, 2nd ed. (Academic Press, San Diego, 1996).

[35] Y. Eliezer, L. Hareli, L. Lobachinsky, S. Froim, and A. Bahabad, Breaking the Temporal Resolution Limit by Superoscillating Optical Beats, Phys. Rev. Lett. **119**, 043903 (2017).

[36] E. Neyra and P. Vaveliuk, Tailoring a sub-diffraction optical focus via a straightforward interferometric approach, J. Opt. **23**, 075604 (2021).

[37] E. G. Neyra, G. A. Torchia, P. Vaveliuk, and F. Videla, Simple interferometric setup enabling sub-fourier-scale ultra-short laser pulses, J. Opt. **24**, 045504 (2022).

[38] M. F. Ciappina, J. Biegert, R. Quidant, and M. Lewenstein, High-order-harmonic generation from inhomogeneous fields, Phys. Rev. A **85**, 033828 (2012).

[39] M. R. Shcherbakov, K. Werner, Z. Fan, N. Talisa, E. Chowdhury, and G. Shvets, Photon acceleration and tunable broadband harmonics generation in nonlinear time-dependent metasurfaces, Nat. Commun. **10**, 1345 (2019).

[40] D. B. Milošević, G. G. Paulus, D. Bauer, and W. Becker, Above-threshold ionization by few-cycle pulses, J. Phys. B: At. Mol. Opt. Phys. **39**, R203 (2006).

[41] J. Park, A. Subramani, S. Kim, and M. F. Ciappina, Recent trends in high-order harmonic generation in solids, Adv. Phys.: X **7**, 2003244 (2022).

[42] M. Berry and S. Fishman, Escaping superoscillations, J. Phys. A: Math. Theor. **51**, 025205 (2018).

[43] E. Ridente, M. Mamaikin, N. Altwaijry, D. Zimin, M. F. Kling, V. Pervak, M. Weidman, F. Krausz, and N. Karpowicz,

Electro-optic characterization of synthesized infrared-visible light fields, Nat. Commun. **13**, 1111 (2022).

[44] H. Alqattan, D. Hui, V. Pervak, and M. T. Hassan, Attosecond light field synthesis, APL Photonics **7**, 041301 (2022).

[45] S.-W. Huang, G. Cirmi, J. Moses, K.-H. Hong, S. Bhardwaj, J. R. Birge, L.-J. Chen, E. Li, B. J. Eggleton, G. Cerullo *et al.*, High-energy pulse synthesis with sub-cycle waveform control for strong-field physics, Nat. Photonics **5**, 475 (2011).

[46] A. Wirth, M. T. Hassan, I. Grguraš, J. Gagnon, A. Moulet, T. T. Luu, S. Pabst, R. Santra, Z. A. Alahmed, A. M. Azzeer, V. S. Yakovlev, V. Pervak, F. Krausz, and E. Goulielmakis, Synthesized light transients, Science **334**, 195 (2011).